International Journal of Advanced Science and Technology
Vol. 29, No. 12s, (2020), pp. 801-815

Aerodynamic Characterization Of Albatross-Inspired Airfoils/Wings

Y. D. Dwivedi[1*], Tushar MS Waykar[1] and LVSS Lohitasya Varun[1]
[1*]*Institute of Aeronautical Engineering, Dundigal, Hyderabad, Telangana, India-500043*
Email:[1]yddwivedi@gmail.com, waykarts10@gmail.com, varunllv16@gmail.com*

Abstract

Flight performance of any air vehicle depends on the shape of the airfoils and wings. Observing the natural fliers, it is observed that albatrosses have one of the best flight performances. These birds can soar thousands of kilometers, without spending much of their own energy. This study investigates the effect of albatross wing airfoil on the aerodynamic performance. The aerodynamic performance analysis is undertaken by taking similar geometry and Reynolds number. In this work first different airfoils like E420, 421, 422, 423 and Gottingen airfoils GOE 174 and 176 were studied. The coordinates of the airfoils were extracted from the existing work of UIUC database and simulated by XFLR- 5. Planform of four models of wings namely Albatross 01, Albatross 02, Delta wing and Rectangular wings were modeled. Flow simulation was done in XFLR-5. The coefficient of lift, coefficient of drag and ratio of the coefficient of lift and drag verses angles of attack were obtained at Reynolds number 100000. The result demonstrated that the lift coefficient of Airfoil E423 was best in E series airfoils and when compared with GOE 176 airfoil, it's found that this airfoil is much superior to E423. The aerodynamic performance (C_L/C_D) of the Albatross 02 wing was found much superior than Delta, Rectangular and Albatross 01 wing. These airfoils results showed that the GOE 174 can be used for cruise and glide performance and GOE 176 airfoil could be used for takeoff, landing and maneuvering performance.

Keywords: *Aerodynamic performance, albatross wing, panel method, XFLR-5, Vortex Lattice Method, Lifting Line Theory*

1. Introduction

Albatross a huge sea bird uses dynamic soaring by removing power from the vertical wind speed gradient. These birds take the advantage of wind gradient which are formed due to interaction amid air and sea to fly thousands of kilometers without beating of the wings [1,2]. Rayleigh observed this bird in 14th century and now the interest of researchers are grown much bigger to get the advantage of natural energy for the soaring of the bird which can be used for the purpose of unmanned aerial vehicles (UAVs) [3]. Albatross are mostly found in southern ocean as the wind velocity found to be more than12 m/s in these areas [4]. All the observations revealed little wing flapping as these birds were not adjusted for flapping air travel due to huge size of the wings and having lean muscles [5]. So the flight of the albatross is not as per kinematics of the wings but depends on the trajectories that can be potentially used for the small fixed wing UAVs. Albatross have been observed to perform a certain patterns in the 15-20m above the sea surface as shown in Fig.1. Numbers of studies related to numerical assessment were performed to get the model of the dynamic soaring applied to UAVs [7-9]. The albatross gain the energy out of the wind gust created by the separation of the flow over the waves [6]. Sachs (2004), has numerically emphasized that the energy increase obtained from the upper turn from windward to leeward as measured the albatross flight to support his results [10].

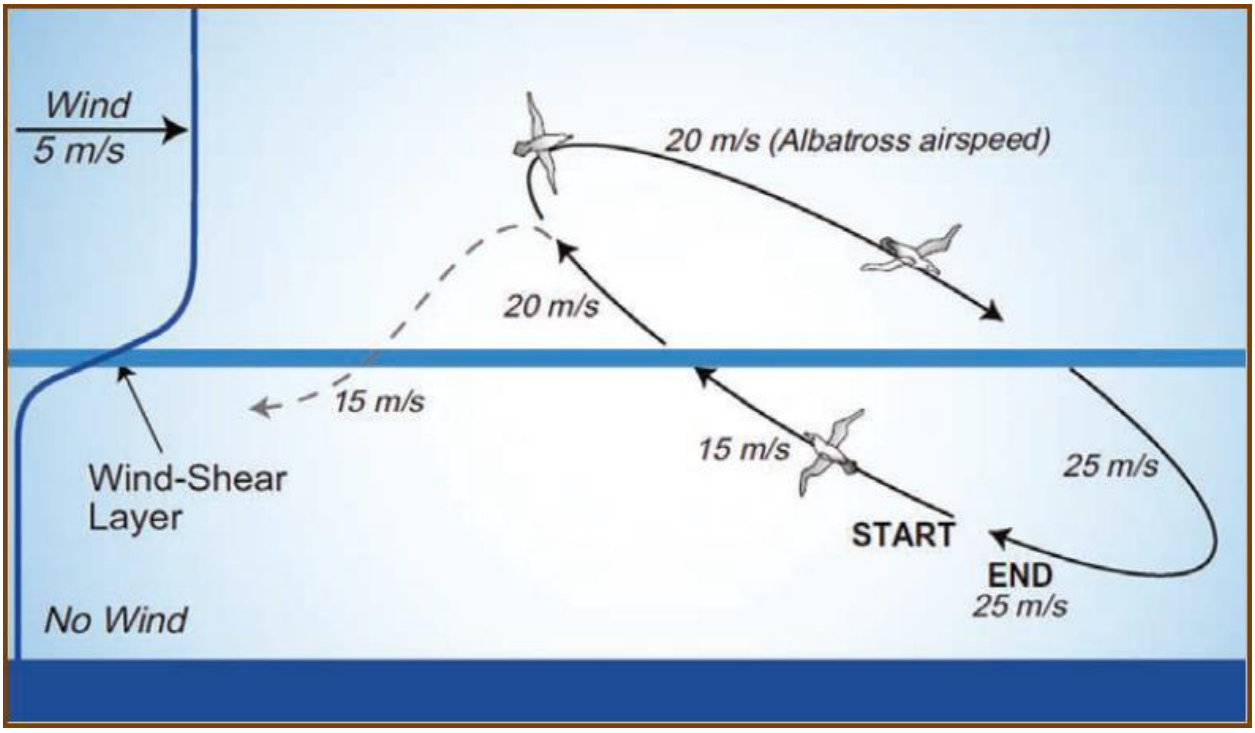

Figure 1. Depiction of dynamic soaring pattern of albatross [6]

A study to investigate the potential of the flight of the albatross to the basis for the UAV wind milling to use for regeneration of the battery power was done [11]. Dynamic soaring (DS) is one of the method to permit aircraft to mine power from the atmospheric wind [12]. So far, the DS has not been focused intensively to estimate path planning and energy variation during DS. Few studies about UAV autonomous soaring flight to understand gliding flight and the path planning was done for autonomous DS in an unknown wind field at sea conditions [13-15]. An estimation of wind field by using polynomial parameterization of the wind field was performed [16]. An adaptive trajectory tracking algorithm was proposed to estimate the aerodynamic characteristics [17].A long distance soaring trajectory for a small UAV to harvest energy from atmospheric wind and prediction of efficient path from the given wind data was proposed [18]. Different researchers have investigated different soaring birds to get physics behind the mechanics of soaring [21] and developed theories to utilize wind gradients for long range and endurance of UAVs flight. A two dimensional (2-D) and three dimensional (3-D) models were made to investigate complete soaring and mass point system for non diving albatross flight [22]. Recent studies were focused on the practical applications of the utilization of the sea wind gradient. These work proposed algorithms and methods for estimating flight trajectory design with high energy harvesting [23-24].Panel method analysis of the bio inspired wing was studied on insect corrugated wings and the results were verified foe low angles of attack in linear range [25-26].

The motive of present article is to assess the aerodynamic performance of the albatross inspired airfoils/wings and compare with the conventional base line wing, which may be useful for the future development of UAVs. These UAVs can be used for the marine surveillance for the navy and coastguard services with minimum power consumption and hence increase the endurance and range of the flight. In this work the prototype wing model was designed with commercial software and simulated by XFLR-5 a 3-D panel method technique. This study is intended to provide a guiding note for the future design aspects to use albatross inspired wings for next generation UAVs.

2. Mathematical formulations

The representation of the normal force applied on every panel of the wing surface:

$$F_i = \rho(\Gamma_i - \Gamma_U)V_i \times \gamma_{12} + \rho(\Gamma_i - \Gamma_R)V_i \times \gamma_{23} + \rho(\Gamma_i - \Gamma_L)V_i \times \gamma_{61} + \rho(\Gamma_U - \Gamma_{UR})V_i \times \gamma_{34} + \rho(\Gamma_U - \Gamma_{UL})V_i \times \gamma_{56}$$

or

$$F_i = \rho(\Gamma_i - \Gamma_U)V_i \times \gamma_{12} + \rho(\Gamma_i - \Gamma_R)V_i \times \gamma_{23} + \rho(\Gamma_i - \Gamma_L)V_i \times \gamma_{61} + \rho(\Gamma_U - \Gamma_{UR})V_i \times \gamma_{34} + \rho(\Gamma_U - \Gamma_{UL})V_i \times \gamma_{56} \quad \text{.....(1)}$$

where ρ represents air density, Γ represents intensity of a vortex ring, V_i the velocity at the panel collocation point and γ is the segment of a vortex line as per geometry.

The representation of the normal force applied on every panel of the wing surface

$$F_i.n_i = \rho\left[n_i \times \left(V_\infty + \sum_{j=1}^{N}\left(\Gamma_j + \Delta\Gamma_j\right)v_{ij}\right)\right].[(\Gamma_i - \Gamma_U)\gamma_{12} + (\Gamma_i - \Gamma_R)\gamma_{23} + (\Gamma_i - \Gamma_L)\gamma_{61} + (\Gamma_U - \Gamma_{UR})\gamma_{34} + (\Gamma_U - \Gamma_{UL})\gamma_{56} + (\Delta\Gamma_i - \Delta\Gamma_U)\gamma_{12} + (\Delta\Gamma_i - \Delta\Gamma_R)\gamma_{23} + (\Delta\Gamma_i - \Delta\Gamma_L)\gamma_{61} + (\Delta\Gamma_U - \Delta\Gamma_{UR})\gamma_{34} + (\Delta\Gamma_U - \Delta\Gamma_{UL})\gamma_{56}] \; (where\ i = 1,2,\ldots,N) \quad \text{.....(2)}$$

V_∞ is the freestream velocity,F_i is the aerodynamic force generated by all the vortex lines placed on the panel, n_i the surface normal vector calculated at the panel collocation point,v_{ij} the velocity induced by the unit strength vortex ring j at the i^{th} panel collocation point andΓ the intensity of a vortex ring

Considering an initial guess value of the given vector $\boldsymbol{X}^0$, the accuracy of this approximation can be improved significantly using the following procedure:

$$\boldsymbol{J}(\boldsymbol{X}^{\boldsymbol{K}})\Delta\boldsymbol{X} = -\boldsymbol{R}(\boldsymbol{X}^{\boldsymbol{K}}) \quad \text{.....(3)}$$

$$\boldsymbol{X}^{\boldsymbol{K}+} = \boldsymbol{X}^{\boldsymbol{K}} + \boldsymbol{\Omega}\boldsymbol{\Delta}\boldsymbol{X}$$

"$J(X^K)$ is the Jacobian matrix of first-order partial derivatives calculated with the current estimate of the solution vector, $-R(X^K)$ the system residual calculated with the current estimate of the solution vector, ΔX the solution increment and Ω an under-relaxation factor. The iterative solutionprocedure continues until the magnitude of the largest residual becomes smaller than the desired convergence criteria" Gabor et al. (2016).

To solve Non-Linear System of Equations, the *Jacobian Matrix* can be computed as four partitions as presented below:

$$\boldsymbol{J} = \frac{\partial \boldsymbol{R}_i}{\partial \boldsymbol{X}_k} = \begin{bmatrix} \frac{\partial\left(-\boldsymbol{F}_i.\boldsymbol{n}_i + \boldsymbol{A}_i.Q_\infty \Delta C_{p,i}^{visc}\right)}{\partial \Delta\Gamma_k} & \frac{\partial\left(-\boldsymbol{F}_i.\boldsymbol{n}_i + \boldsymbol{A}_i.Q_\infty \Delta C_{p,i}^{visc}\right)}{\partial V_k^T} \\ \frac{\partial\left(\sum_{j=1}^{N} \boldsymbol{v}_{ij}.\boldsymbol{n}_i \Delta\Gamma_j + V_i^T\right)}{\partial \Delta\Gamma_k} & \frac{\partial\left(\sum_{j=1}^{N} \boldsymbol{v}_{ij}.\boldsymbol{n}_i \Delta\Gamma_j + V_i^T\right)}{\partial V_k^T} \end{bmatrix} \quad \text{.....(4)}$$

"A_i is the area of the panel and Q_∞ is the dynamic pressure of the free stream.v_{ij} the induced velocity created by the unit strength vortex ring j at the i^{th} panel collocation point $\Delta C_{p,i}^{visc}$ represents the viscous pressure coefficient distribution V_i^T represents the modulus of the surface transpiration velocity,F_i is the aerodynamic force generated by all the vortex lines placed on the panel, n_i the surface normal vector calculated at the panel collocation point and Γ the intensity of a vortex ring". All these equations are obtained from Gabor et al. (2016) [27].

3. Methodology

3.1 Airfoil geometry selection

All the airfoils data which are used in this work are imported from the University of Illinois at Urbana-Champaign (UIUC) airfoil coordinated database includes airfoils, and covers variety of applications. This database contains files in DAT format, the DAT file contains the coordinates which are used in XFLR5. These data base also have GIF files, which helps to visualize the contour of the airfoil. Using direct foil design option in XFLR5, the software generates the airfoil contour/profile. The XFLR 5 is able to manage airfoils by changing its cambered, thickness, and other geometric parameters. Also, we can interpolated two airfoils to make new one which is having both parent airfoil's characteristics primary requirement to make a wing to carry maximum weight. To get high payload fraction (ratio of payload weight to takeoff weight), the airfoil which are having high lift to drag ratio (aerodynamic performance, Cl/Cd) such as E420, E421, E422, E423 are studied. Out of which Eppler 423 is selected for its good performance at low Reynolds number (Re). The maximum thickness (t_{max}) of Eppler 423 is increased from 12% to 15% to get thick airfoil which can be fabricated easily due to high thickness. Selected e423 airfoil is further compared with conventional albatross airfoils which are GOE 174 and GOE 176. These airfoil sections are shown in figure 2 and 3 respectively.

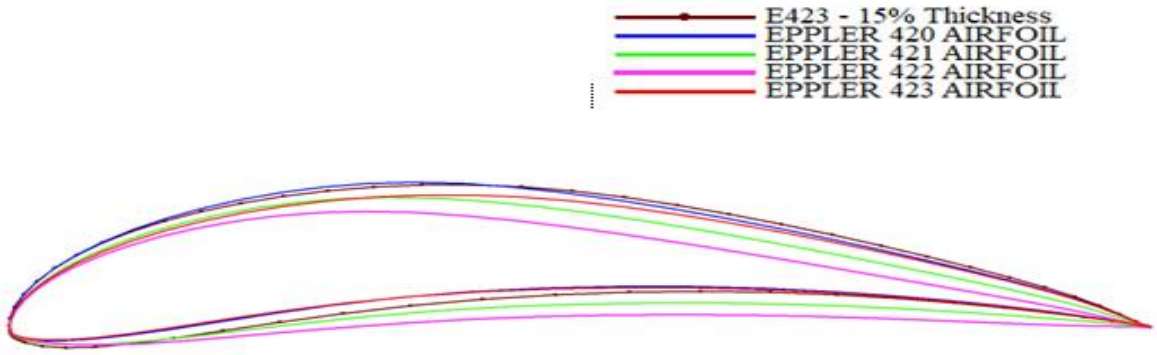

Figure 2. Eppler 420, 421, 422, 423 and Eppler 423 with 15% thick airfoil

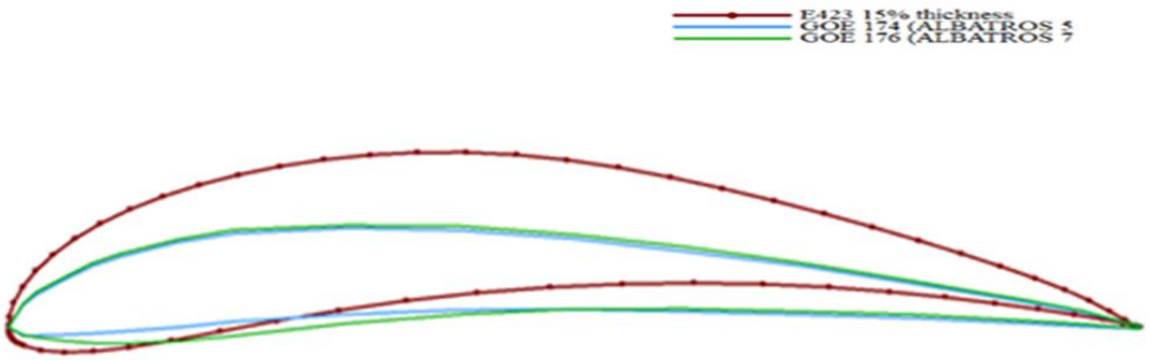

Figure 3. Eppler 423-15% thick, GOE 174 and GOE 176 albatross wing airfoil

3.2Wing configuration

Various types of wing shapes of different bird having high L/D ratio are observed and examined in detailed as shown in table 1, the Aspect Ratio and Wingspan was fixed for the Multi - Taper Main wing (Albatross 01). Appropriate dihedral was given by identifying weak points in Structure of wing and suitable to perfect aerodynamic shape. Much of the swept back was inspired by high soaring birds during their glide flight. Selected wing planform is applied or fixing to the fuselage at different locations and different ways of swept. Final selection goes with wing which fulfills all the requirements. Different types of wing planform like Conventional albatross (Albatross 01, 02), delta and rectangular having same span, aspect ratio, wing area are created and analyzed. The dimensions are given in table 2 and all wing planform are shown in figure 4.

Table 1. Different Bird wing Configuration

Type	**Figure of Merit**
Bird Type (Wing Structure)	Falconidae (Falcons)
	Diomedeidae (Albatross)
	Gannets (Morus)
	Gulls (Larus)
Wing planform	Swept
	Tapered
	Rectangle
Wing location	High
	Middle
	Low
Parameter	**Main Wing**
Wing span	0.88m
Wing surface area	$0.0903m^2$
Aspect ratio	8.576
Root chord	0.15m
Taper ratio	2.5

Sweep angle	12.49^0
Mean aerodynamic chord	0.10853m

Table 2. Wing geometrical dimensions

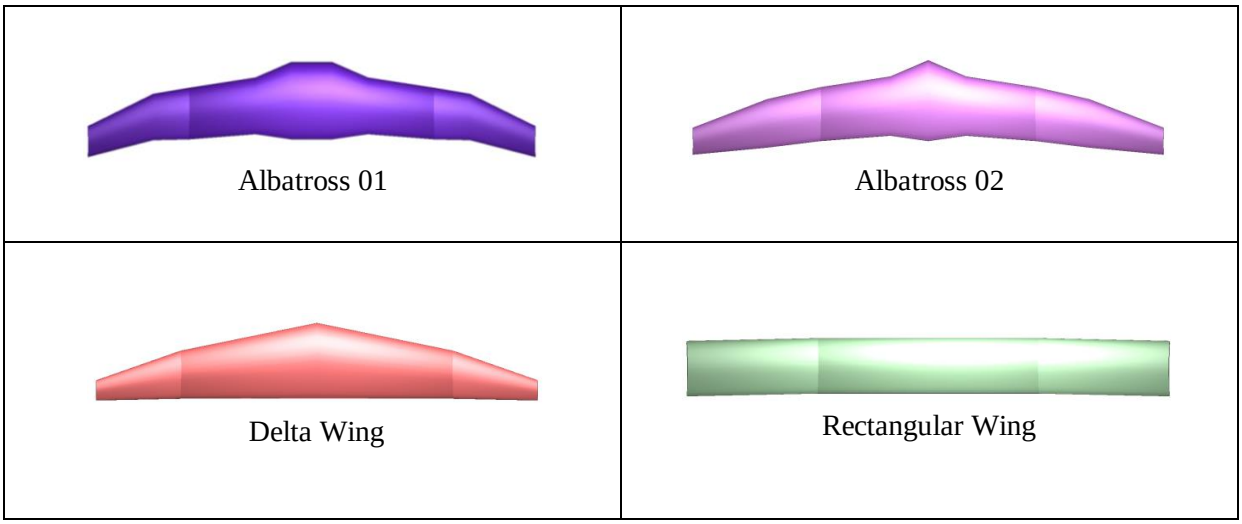

Figure 4 Different wing planform

4. Results and analysis

All the analysis is performed in XFLR 5-V6 software which is also able to handle viscous and non linear effect. The aerodynamic analysis of airfoils and wing planform like coefficient of lift (C_l), coefficient of drag (C_d) and ratio of lift to drag coefficients (C_l/C_d) versus angle of attack (AOA) is performed by using Ring Vortex Lattice Method known as VLM 2 in XFLR5 -V6. The analysis is carried out by using Reynolds number up to 1,00,000, which corresponds to the velocity of 20 ms^{-1}. Ground effect up to 50 m is considered. Viscous effect is considered for airfoil and wings analysis. Ring Vortex Lattice Method (VLM 2) is applicable to any shape of wing as they considered dihedral and swept angles and also viscous and non linearity is handled. In VLM, lift coefficient, moment coefficient, center of pressure's position and induced drag which is linear and inviscid is calculated. In ring vortex lattice method (VLM 2), trailing vortices are extended to infinity. VLM method solves the Laplace equations for an airfoil and wing following a typical action using rings of the vortex as the main elucidation. The rings are situated at the quarter chord ($1/4^{th}$ of c) of geometric panels on the wing's curvature facade (bound vortex rings), as well as in the wake vortex rings. Vortex rings are also made to locate in the wake so that the simulation of the free vortex sheet can be done easily. The Kutta condition is implemented at the trailing edge where the flow is assumed to be separated. This is enforced by shedding the vorticity of the bound trailing edge panels with the intention of model the leading edge flow separation.

4.1 Coefficient of pressure (Cp) distribution over the wings

The pressure coefficient is defined as a dimensionless quantity of the pressure difference (pressure difference divided by dynamic pressure). When the pressure is measured on upper surface of an airfoil, it's the difference of pressure with ambient pressure. The values of this can be positive or negative as per flow conditions. The Cp results of four wings are shown in figure 5. These results show that the Albatross 01 wing produces lesser negative Cp in upper surface than the Albatross 02 wing. The Albatross 02 wing produces negative value of Cp on upper surface of the wing. This wing produces much lift than the albatross 01, Delta wing and rectangular wing as the intensity of Cp on Albatross 02 wing is much higher than all other tested three wings. It is also to mention that the

rectangular wing produces, least negative Cp on the upper surface and hence least lift coefficient. The results also demonstrate the distribution of lift coefficient in spanwise direction pointing upwards and drag coefficient distribution in x direction parallel to the flow. It can be seen from the figure 5 of albatross 02 that the lift coefficient is approximately elliptical and drag coefficient distribution is pretty smooth from tip to root of the wing; however in other wing configurations the lift curve is not elliptical and drag curve is not smooth having highest zig-zag distribution in albatross 01 wing, followed by delta wing and rectangular wing. Observing the lift coefficient distribution, it is observed that the lift coefficient is quite smooth in rectangular wing and significant zig-zag in Albatross 01 wing. The pattern of delta wing is similar to Albatross 02 wing except that the Albatross wing produces more lift towards the tip also than the delta wing. The Cp, C_l and C_d of Albatross wing is found much better than other tested wings in this work.

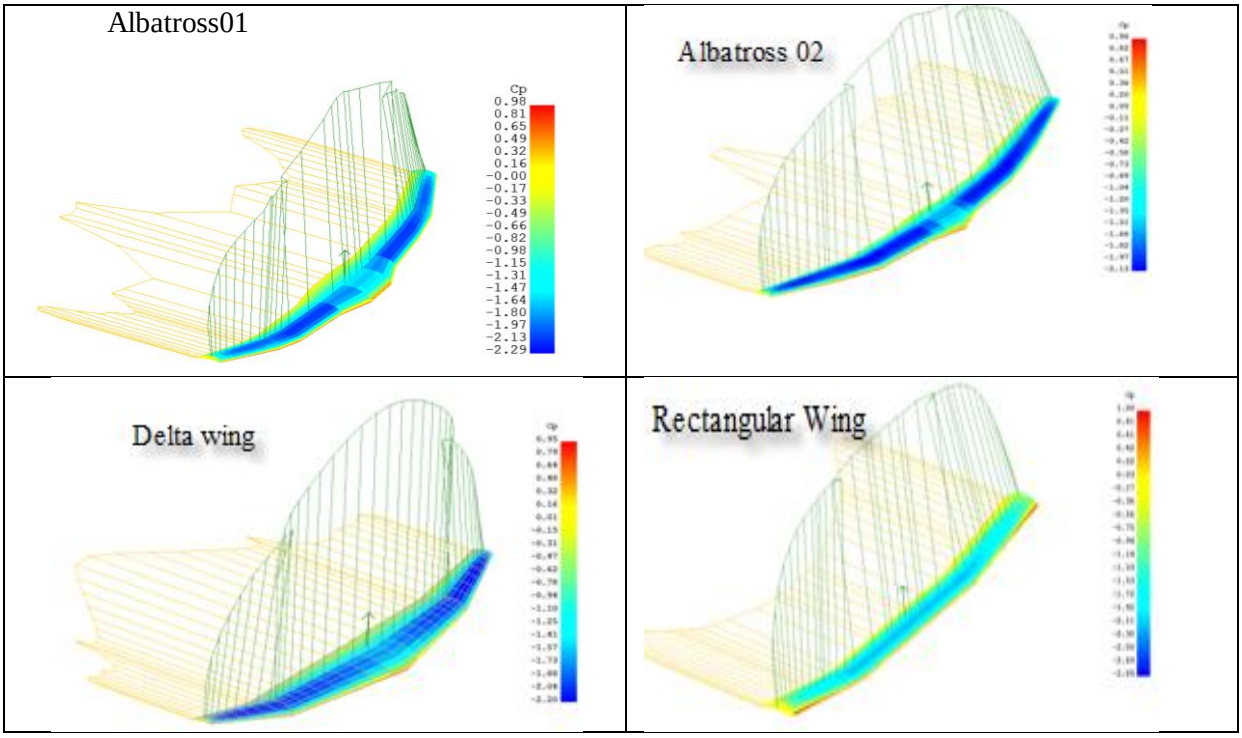

Figure 5. Coefficient of pressure (cp) distribution, lift and Induced drag analysisof four tested wings

4.2 Aerodynamic analysis of E420, E421, E422 and E423 airfoils

Results of lift coefficient (Cl) with variation of angle of attack (AOA) for the four airfoils E420, E421, E422 and E423 is shown in figure 5. Result shows that, for the negative AOA, Airfoil E420 gives best lift coefficient of 0.5 followed by Airfoil E423, E422 and E421. However, in positive AOA Airfoil E423 outperformed the remaining three tested airfoils upto stall angle i.e. 20 degree followed by E420, E422 and E421. There is significant difference in maximum lift coefficient between E423 and E422 which is 24%. Another important result is that the Cl of Airfoil E423 and E420 fall sharply beyond the stall angle and in other two airfoils E421 and E422, the stall angle not achieved till tested 26^0 AOA. So, the E421 and E422 airfoils can be used for much higher stall AOA without loss of lift.

Another important aerodynamic characteristic is drag coefficient. The Cd of the airfoil E421 is highest and E420 is lowest among other tested airfoils in negative angles of attack. At positive AOA from 0 to 27^0, Airfoils E421 and E422 produce lowest drag in comparison with E420 and E423. The highest drag is produced by airfoil E420 at all positive AOA and a sharp increase of drag observed in this airfoil at 26^0 AOA, which is not suitable beyond this AOA. At 6^0 AOA, the

difference in drag coefficient between airfoil E420 is 80% more than Airfoil E421/422. At 20 ^{0} AOA, this difference in drag coefficient comes down to 30%. So the Airfoils E421/422 are suitable for lower AOA upto 10^0 (Fig.7).

Aerodynamic performance is defined by the ratio of lift to drag coefficient. The plot of C_l/C_d for the four tested airfoils is shown in figure 8. At negative AOA, Airfoil E420 performed better. However, at positive AOA, this airfoil aerodynamic performance falls and is least among all airfoils. Considering positive AOA, the Airfoil E422 is the best, where L/D ratio is 25 at 6^0 AOA Followed by E421, E423 and E420. Here it is also to be notices that the airfoil E421 can work for more AOA upto 10^0 and the range is from 6 to 10 degrees AOA. So if we want to use the airfoil E422 beyond 6^0 AOA, it's not efficient and E421 can give better performance upto 10^0 AOA.

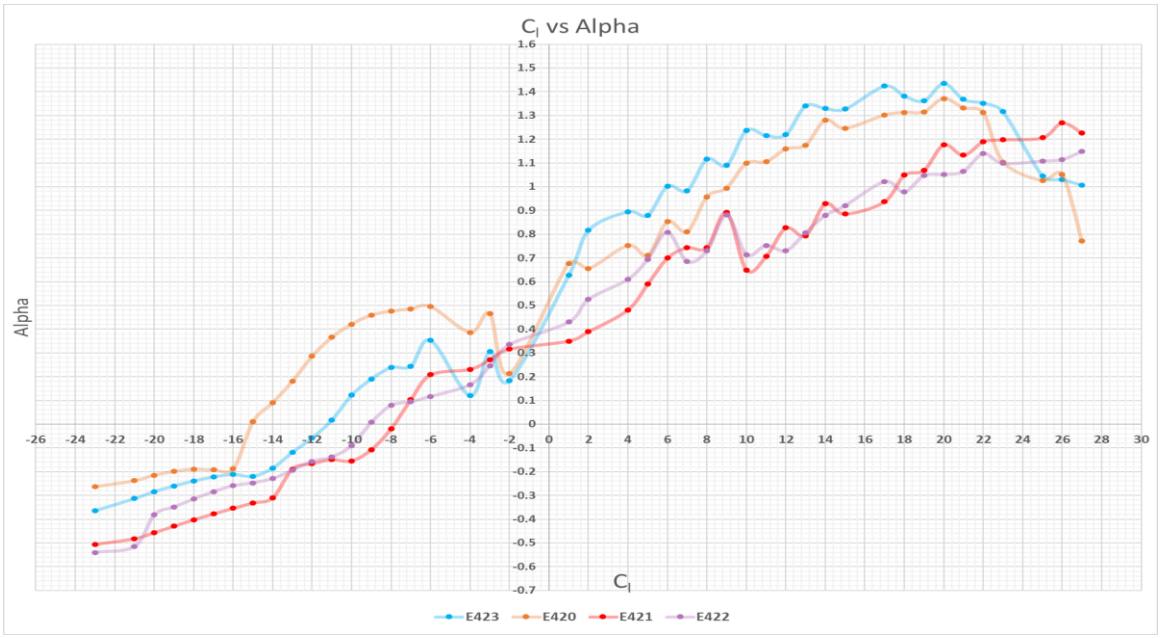

Figure 6. C_l verses AOA for E423 over E420, E421, E422 airfoils

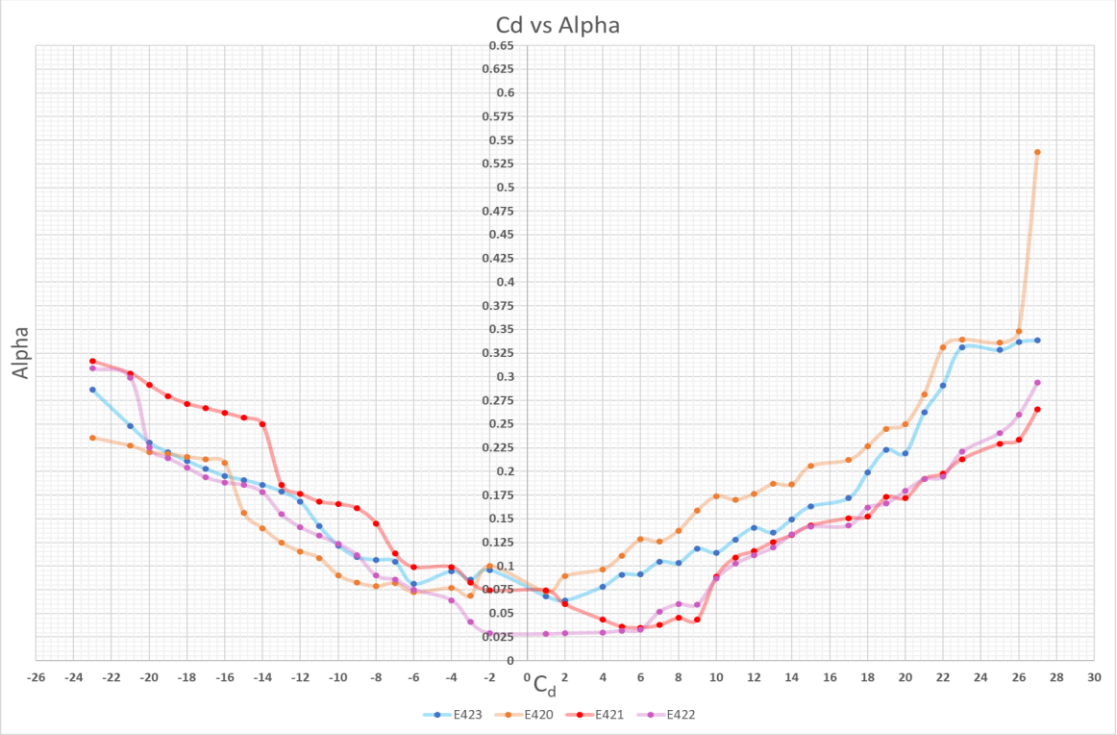

Figure 7. C_d verses AOA for E423 over E420, E421, E422 airfoils

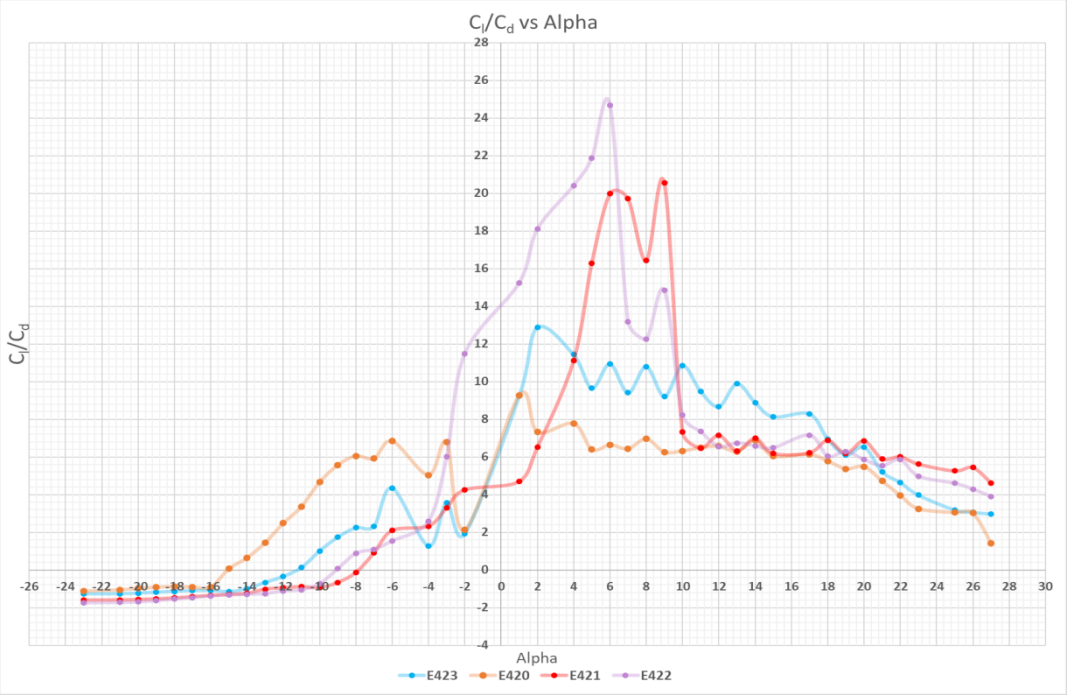

Figure 8. Ratio of Coefficient of lift/ drag verses AOA for E423 over E420, E421, E422 airfoils

4.3 2-Dimensional aerodynamic comparison of modified E423 airfoil with conventional albatross airfoils GOE174 & GOE176

In this section three airfoils E423, GOE 174, and GOE 176 are compared with vortex lattice method 2 (VLM2) by using XFLR -5. The GOE 174 (ALBATROS 5020) airfoil having maximum thickness 8.6% at 19.9% chord, maximum chamber 5.6% at 39.9% of chord. The GOE 176

(ALBATROS 7020) air foil having maximum thickness of 10.3% at 19.8% of chord with maximum chamber 5.6% at 39.8% chord (source -UIUC).The Cl verses AOA plot for the three airfoils are shown in figure 9. The GOE 174 airfoil produces positive lift coefficient from -12^0 AOA onwards and the maximum C_l of 1.45 is found at 3^0 AOA. This angle is stall angle and C_l falls significantly. The GOE 176 airfoil does not produce positive lift at negative AOA. The maximum C_l of 1.45 is obtained at 15^0 AOA, which is equal to GOE174, with Stall angle of GOE 176 is significantly higher than the GOE 174 which is 3^0. The E423 (15% increase in thickness) airfoil produces positive C_l from -13^0 AOA and having zig-zag C_l curve everywhere and having stall angle of 20^0. So out of these airfoils the two GOE174 and 176 are having maximum C+ of 1.45 with stall angle 3 and 15 degrees respectively. However, the modified E423 airfoil has comparatively higher stall angle than another two airfoils investigated.

The GOE 174 airfoil produces lower drag than the GOE 176 and modified E423 airfoils at all negative tested AOA. At positive AOA higher than 8^0, the sharp increase in Cd is found. This airfoil produces least drag of 0.025 from -8 to +3 degrees AOA. So this airfoil is most suitable in this range of flight AOA operations as in this range this airfoil consume least power from power source. GOE176 produces high C_d at negative AOA, however at positive AOA, this airfoil produces least C_d upto all tested positive AOA. Special feature of this airfoil is that it produces least C_d for all positive AOA compared to GOE 174 and modified E423. This airfoil is the most suitable airfoil when the aircraft operates in the positive AOA ranges from 0-15 degrees as in his range the C_d is less than 0.05. E423 airfoil produces high C_d at all negative AOA and also in positive AOA produces higher C_d than the GOE 176, 174 and not suitable for any flight conditions compared to GOE 174 and GOE 176.

A plot of C_l/C_d versus AOA plot is sown in figure 11. This plot shows that the GOE 174 and GOE 176 both have same C_l/C_d of approximately 56. However, there is a significant difference in the operating range of these two airfoils. The GOE 174, produces higher value of C_l/C_d at low AOA i.e. -3 to +3 degrees. Another GOE 176 airfoil produces same C_l/C_d as GOE 174 but the operating range of this airfoil is positive AOA from +7 to +13 degrees. These both GOE airfoils produce higher value of C_l/C_d than the modified E423 airfoil. However, at high AOA ($>25^0$), modified E423 airfoil improves aerodynamic performance than at lower AOA. Ai negative AOA, the E423 airfoil performs better than the GOE 176 airfoil.

These results indicate that the GOE174 series airfoil can be used for maximum range and endurance during cruise and glide flight conditions. The GOE 176, which performs better at high AOA, can be used for the takeoff, landing and maneuvering flight conditions.

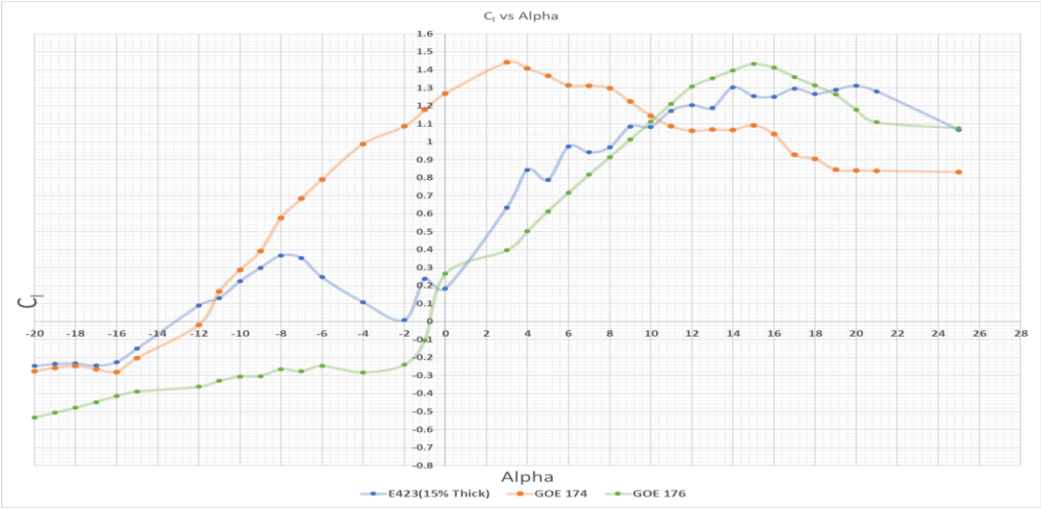

Figure 9. C_l verses AOA for E423, GOE174 and GOE 176 airfoils

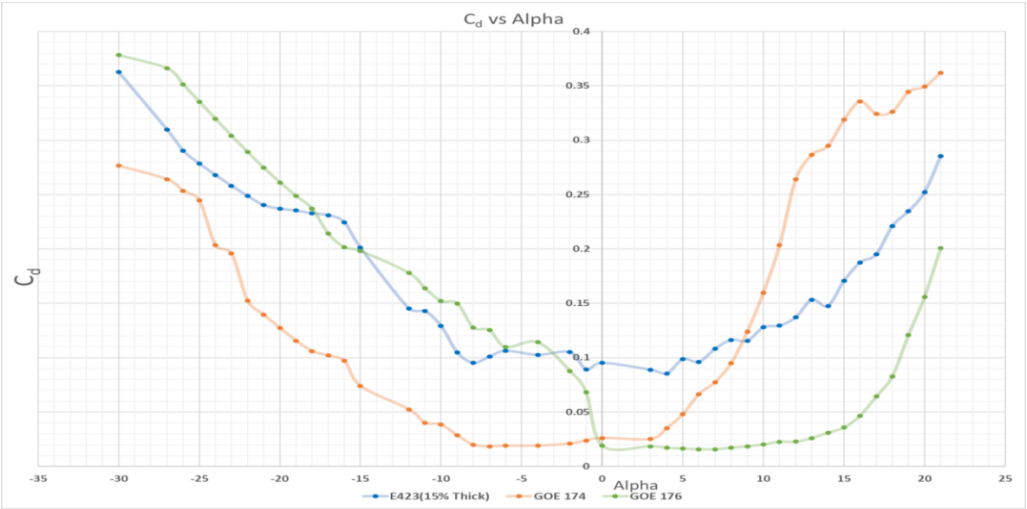

Figure 10. C_d verses AOA for E423, GOE174 and GOE 176 airfoils

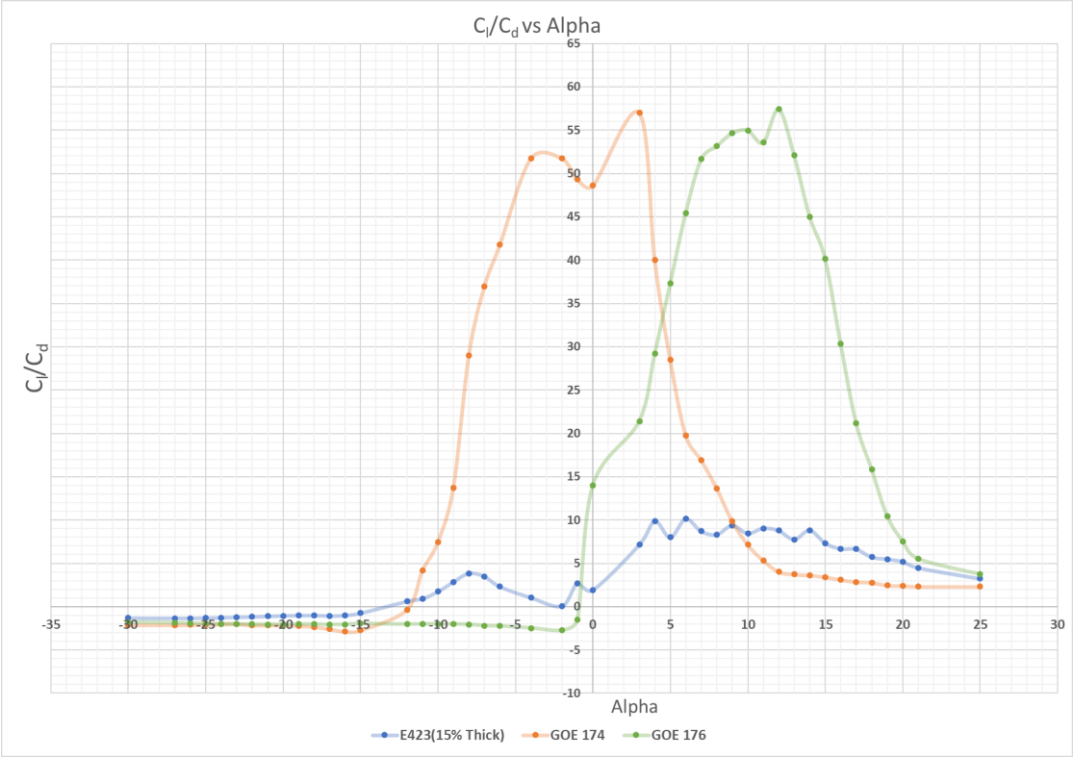

Figure 11. C_l/C_d verses AOA for E423, GOE174 and GOE 176 airfoils

4.4 3-Dimentional aerodynamic characteristics comparison among albatross 01, albatross 02, delta wing and rectangular wings

In this section four 3-D wings namely albatross 01, albatross 02, delta wing and rectangular as shown in figure 5 are analyzed by using vortex lattice method 2 (VLM-2). The E423 modified airfoil with increase in thickness by 15% is used for all the four wings. It was noticed that the C_l of the albatross 02 wing was minutely higher than the other wings at higher AOA. The Cl of rectangular wing was found lowest among all other wings as shown in figure 12. The C_l of the delta wing is somewhat better than the rectangular wing. However the lift coefficients of the both albatross wings are much better than the delta and rectangular wings.

The drag coefficient of the albatross wing 02 found lower than other three tested wings at -12 to +20 degree AOA. However the drag coefficient of albatross 01 wing is found higher than tested other wings. The delta and rectangular wings drag comes between the two (Fig.13).

The aerodynamic performance (C_l/C_d) of Albatross 02 wing was found highest (27) nearly -7 degree AOA followed by Albatross 01 (24), Delta wing (21), and Rectangular wing (18) at -7 degree AOA. This shows that the Albatross o2 wing performed better aerodynamically than other three tested wings planform (Fig.14)

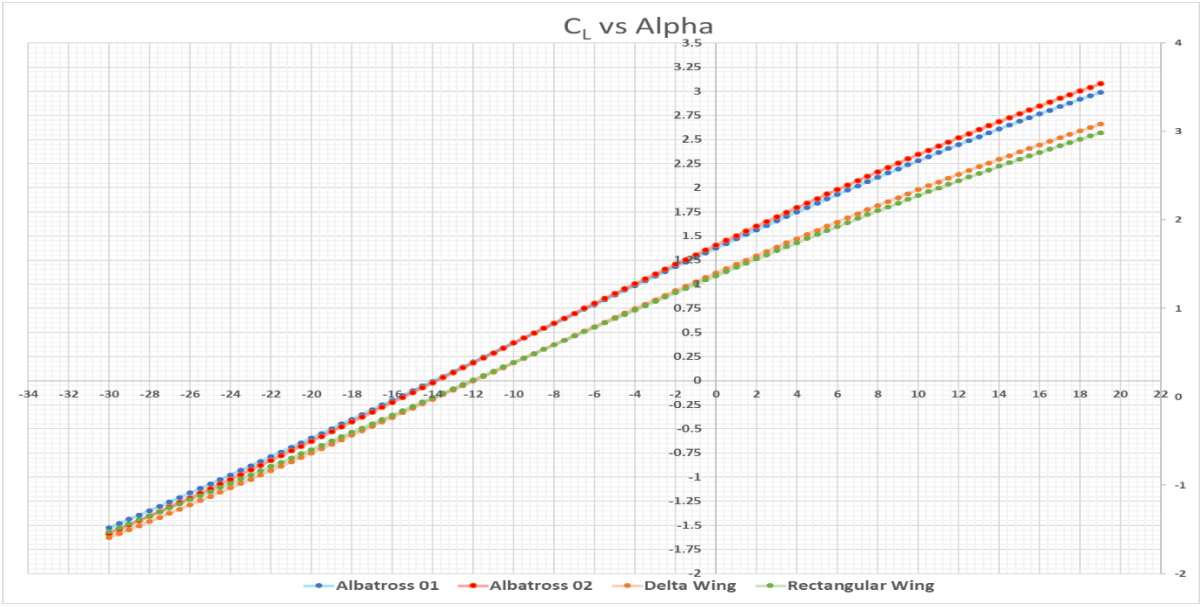

Figure 12. Comparison of C_l verses AOA for different tested wings

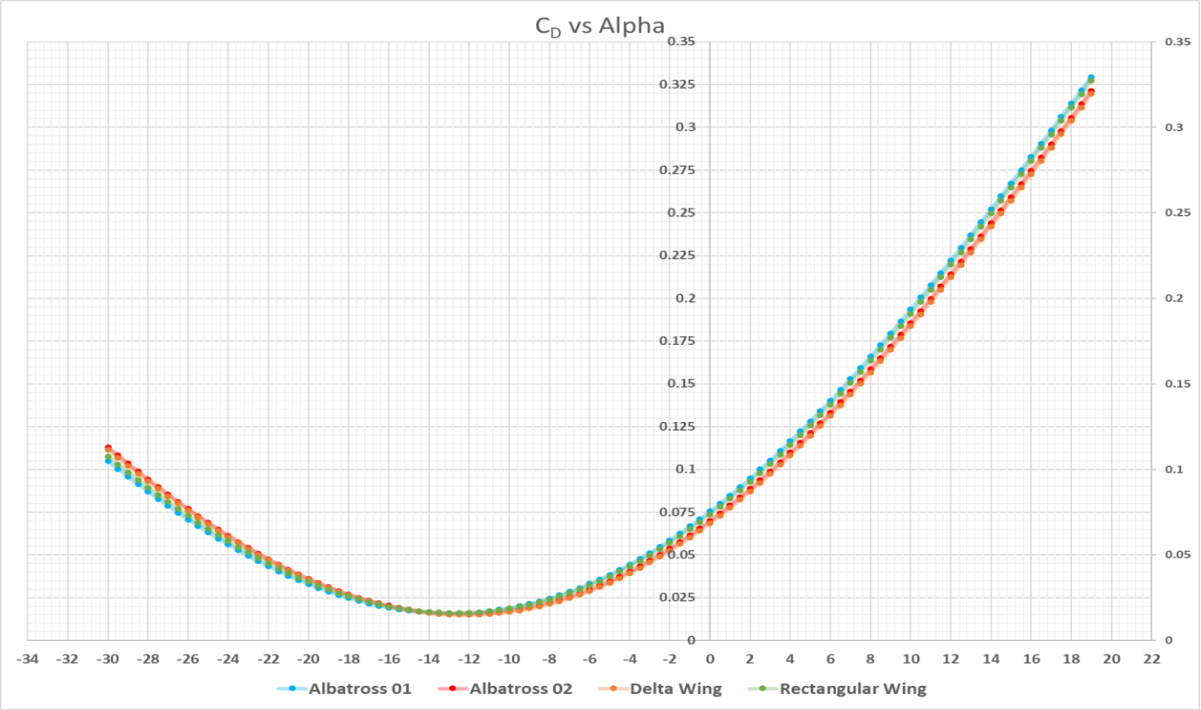

Figure 13. Comparison of C_d verses angle of attack for different wings

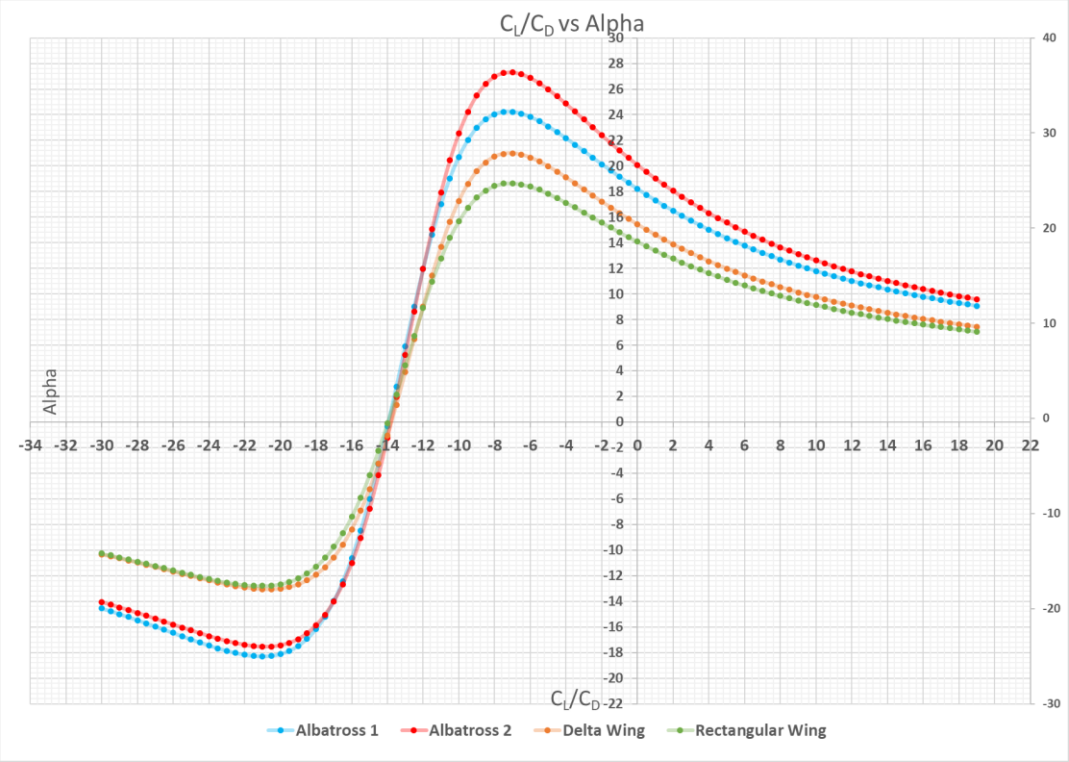

Figure 14. Comparison of C_l/C_d verses AOA for different wings

5. Conclusions

2-D aerodynamic characteristic analysis of the different airfoils such as E420, E421, E422 and E423 and another group of 2-D airfoils like modified E423, GOE 174 and GOE 176 and also 3-D analysis of four different wing planform like Albatross 01, Albatross 02, Delta wing, and Rectangular wing were undertaken by vortex lattice method at Reynolds number 100000 with speed 20 ms^{-1}. The main conclusions are:

1. Lift coefficient of E423 was the best in comparison with E420, E421 and E422. The drag coefficient (C_d) of E422 was least among other airfoils. However, the drag coefficient of E423 found in between E420 and E421 airfoils. The aerodynamic performance (C_l/C_d) of E422 was the best upto 6 degrees AOA. The airfoil E421 demonstrated the best aerodynamic performance at higher positive angles of attack ranging from 6 to 10 degrees.
2. Lift coefficient of GOE 174 was found higher than GOE 176 and E423 from -12 to +10 degree AOA. However, the lift coefficient of GOE 176 was found highest at positive AOA from +10 to +18 degree AOA and not efficient at negative AOA. Drag coefficient of GOE 174 is the least at all negative angles of attack and upto + 8 degrees. GOE 176 produced least drag at all positive angles of attack. The aerodynamic performance of GOE 174 was the best at -13 to +5 degree AOA and at positive higher AOA the GOE 176 airfoil outperformed GOE 174 and E423 airfoils. These airfoils results shows that the GOE 174 can be used for cruise and glide performance where albatross fly and GOE 176 airfoil can be used for takeoff, landing and maneuvering performance.
3. The aerodynamic performance (C_l/C_d) of the four types of undertaken by XFLR-5, the result shows that the Albatross 02 wing performed better than Delta wing, Rectangular wing and Albatross wing 01. This results shows that the GOE 176 can be used for the micro air vehicles by taking the advantages of dynamic wind soaring over the sea.

This work will be useful for future development of the MAV/UAV by using albatross like wings so that it can fly for long time by using nature available energy.

References

1. A.Chakrabarty, and J.W. Langelaan. 2010. "Flight Path Planning for UAV Atmospheric Energy Harvesting using Heuristic Search." Guidance Navigation and Control Conference. AIAA . pp. 1-18.
2. C.J.Wood. 1925. "The Flight of Albatrosses (a Computer Simulation),." IBIS , Vol 115 pp. 244-256.
3. C.Pennycuick. 2008. Modelling the Flying Bird (Theoretical Ecology Series).
4. C.Wood. 1973. "The Flight of Albatrosses (A Computer Simulation)." IBIS pp. 115, 244-256.
5. F.Hendriks "Dynamics Soaring in shear flow (of gliders)." In Proceedings of the 2nd International Symposium on the Technology and Science of Low Speed and Motorless Flight. Cambridge, MA, USA (1974) Sept 11-13.
6. G.C.Bower. n.d. Boundary Layer Dynamic Soaring for Autonomous AIrcraft : Aircraft Design and Validation. Phd Thesis, Stanford University: Stanford.
7. G.K.Taylor, K.V.Reynolds, and A.L.R.Thomas. 2016. "Soaring Energetics and Glide Performance in a moving Atmosphere." Philosophical Transactions of Royal Society B pp. 371.
8. G.Sachs. 2004. "Minimum shear wind strength required for dynamic soaringof Albatrosses." Ibis, Vol. 147, No. 1 pp. 1-10.
9. H Holzapfel, J. Traugott, and G. Sachs. 2011. "Progress against the wind with Dynamic Soaring Results from In-Flight Measurement of Albatrosses." AIAA Guidance Navigation and Control Conference AIAA 2011-6225. AIAA.
10. H.Weimersketch, T.Guionnet, J.Martin, S.A.Shaffer, and D.Costa. 2000. "Fast and Fuel Efficient? Optimal Use of WInd by Flying Albatrosses." Proceedings of the Royal Society B Biological Sciences. London. pp. 1869-1874.
11. J.L.Nguyen, N.R.J.Lawrance, R.Fitch, and S.Sukkarieh. 2016. "Real-Time path planning for long-term information gathering with an aerial glider." Auton.Robots pp. 40, 1017-1039.
12. J.W.Langelaan, J.Spletzer, C.Montella, and J.Grenestdt. 14-18 May 2012. "Wind Field Estimation for Autonomous Dynamics soaring." In Proceedings of the IEEE International COnference on Robotics and Automation (ICRA). St.Paul, MN, USA: IEEE. pp. 16-22.
13. L.Rodriguez, J.A.Cobano, and A.Ollero "Wind Field estimation and Identification having shear wind and discrete gusts features with a smal UAS." In Proceedings of the IEEE/RSJ International Conference on Intelligent Robots and Systems (IROS) . Daejeon, Korea: IEEE. pp. 5638-5644. 2016, October 9-14
14. M.Deittert, A.Richards, C.Toomer, and A.Pipe. 2009. "Engineless Unmanned Aerial Vehicle Propulsion by Dynamic Soaring." Journal of Guidance, Control and Dynamics, Vol. 32, No. 5 pp. 1446-1454.
15. M.Denny. 2008. "Dynamic Soaring : Aerodynamics for Albatrosses." European Journal of Physics 30, 75.
16. M.Rosen, and A.Hedenstorm. 2001. "Gliding Flight in a Jackdaw : A Wind Tunnel Study." The Journal of Experimental Biology pp. 204, 1153-1166.
17. N.D.Liu, Z.X.Hou, Z.Guo, X.X.Yang, and X.Z.Gao. 2016. "Bio-inspired energy-harvesting mechanisms and patterns of dynamics soaring." Bioinspiration & Biomimetics 12. 016014.
18. N.K.Long, and S.Watkins. 22-23 November 2018. "Bio-inspired Regenerative Flight Trajectory Optimization Over Flat Topography." 10th International Micro Air Vehicle Conference. Melbourne, Australia.
19. N.R.J.Lawrance. 2011. "Path Planning for Autonomous Soaring Flight in Dynamic Wind Fields." International Conference on Robotics and Automation. IEEE. pp. 2499-2505.
20. N.R.J.Lawrance, and S.Sukkarieh. 2009. "A Guidance and Control Strategy for Dynamic Soaring with a Gliding UAV." International Conference on Robotics and Automation. IEEE. pp. 3632-3637.
21. N.R.J.Lawrance, and S.Sukkarieh. 2011. "Autnomous Exploration of a Wind Field with a Gliding Aircraft." Journal of Guidance, Control and Dynamics, Vol.34 pp. 719-723.
22. V.A.Tucker, and G.C.Parrott. 1970. "Aerodynamics of Gliding Flight in a falcon and Other Birds." The Journal of Experimental Biology pp. 345-367.
23. Y.Zhao. 2004. "Minimal Fuel Powered Dynamic Soaring of Unmanned Aerial Vehicle utilizing wind gradients." Optim. Control. Appl Meth, Vol. 25 pp. 211-233.

24. Z.Y.Zuo. 2013"Adaptive Trajectory Tracking Control Design with command Filtered Compensation for a Quadrotor." Journal of Vibration and Control, Vol. 19 pp. 94-108.
25. Y.D Dwivedi,and V. Bhargava. 2019. "Aerodynamic charecterization of bio inspired corrugated wings". MOJ App Bio Biomech Vol 3 (1). pp1-10
26. Y. D. Dwivedi, 2018, " Aerodynamic performance and stability analysis of bio inspired corrugated wings for micro air vehicle" phD Thesis, VFSTR University Guntur, AP India.
27. O.S. Gabor, K. Andreai, & R. M. Botez. 2016. A new non-linear vortex lattice method:Applications to wing
a. aerodynamic optimizations. Chinese Journal of Aeronautics, pp. 4-6. doi:http://dx.doi.org/10.1016/ j.cja.2016.
b. 08.001